Anomalous small angle x-ray scattering determination of ion distribution around a polyelectrolyte biopolymer in salt solution

Ferenc Horkay
Section on Tissue Biophysics and Biomimetics, Laboratory of Integrative and Medical Biophysics, NICHD, National Institutes of Health, Bethesda, Maryland 20892

Anne Marie Hecht and Cyrille Rochas
Laboratoire de Spectrométrie Physique, CNRS UMR 5588, Université J. Fourier de Grenoble, B.P. 87, 38402 St Martin d'Hères Cedex, France

Peter J. Basser
Section on Tissue Biophysics and Biomimetics, Laboratory of Integrative and Medical Biophysics, NICHD, National Institutes of Health, Bethesda, Maryland 20892

Erik Geissler[a)]
Laboratoire de Spectrométrie Physique, CNRS UMR 5588, Université J. Fourier de Grenoble, B.P. 87, 38402 St Martin d'Hères Cedex, France

(Received 21 August 2006; accepted 6 November 2006; published online 20 December 2006)

The distribution of counterions in solutions of high molecular mass hyaluronic acid, in near-physiological conditions where mono- and divalent ions are simultaneously present, is studied by small angle neutron scattering and anomalous small angle x-ray scattering. The solutions contain either sodium or rubidium chloride together with varying concentrations of calcium or strontium chloride. The effects of monovalent-divalent ion exchange dominate the amplitude and the form of the counterion cloud. In the absence of divalent ions, the shape of the anomalous scattering signal from the monovalent ions is consistent with the distribution calculated from the Poisson-Boltzmann equation, as found by other workers. In mixtures of monovalent and divalent ions, however, as the divalent ion concentration increases, both the diameter and the amplitude of the monovalent ion cloud decrease. The divalent counterions always occupy the immediate neighborhood of the charged polyanion. Above a given concentration their anomalous scattering signal saturates. Even in a large excess of divalent ions, ion exchange is incomplete. © *2006 American Institute of Physics*.
[DOI: 10.1063/1.2402921]

INTRODUCTION

Hyaluronic acid (HA), a copolymer of *N*-acetyl-D-glucosamine and D-glucuronic acid, is a high molecular weight hydrophilic polysaccharide. It has a number of biological roles. HA is a major contributor to the biomechanical properties of tissues, controls tissue hydration and water transport, influences the lubrication and viscoelastic properties of synovial fluid, serves as the structural backbone of cartilage proteoglycan assemblies, and plays a role in skeletal formation.[1–4]

HA is a stiff polymer, owing mainly to hydrogen bonds that connect the neighboring residues.[5] Long range electrostatic (Coulomb) repulsion favors an extended conformation. In the physiological environment HA exists almost exclusively in sodium salt form. HA is widely distributed in connective tissue and may have important effects on the distribution of ions within the body fluids, notably as an ion exchange medium. Biomechanical and hydrodynamic studies have been made as a function of the ionic strength on HA solutions, but these investigations do not address the distribution of counterions.[6–8] In view of the role played by the counterions in the above-mentioned functions, it is of importance to determine the ion distribution around the HA molecule in a near-physiological ionic milieu, i.e., in excess salt conditions in which both monovalent and divalent cations may simultaneously be present.

Much of the current understanding of the effect of ions is based on molecular dynamics modeling. These simulations have shown that in the presence of divalent counterions, short-range attractive interactions with clustering and domain formation arise.[9,10] Simulations and density functional theory calculations also indicate that the spatial extent of the counterion cloud for highly charged rod polymers is significantly reduced in the case of divalent counterions relative to monovalent counterions.[11,12]

Monovalent counterions form a cloud surrounding the chain, and at higher ion concentration (i.e., when the distance between neighboring charged groups is smaller than the Bjerrum length, 7.1 Å), a fraction of these ions is believed to adsorb on the macroion.[13] Many studies indicate that the distribution of monovalent ions can be approximated by the Poisson-Boltzmann (PB) theory.[14–16] This theory, however, does not describe the counterion atmosphere in the presence of divalent ions,[17,18] such as the calcium ions that are generally present in natural physiological environments. The PB

[a)]Electronic mail: erik.geissler@ujf-grenoble.fr

theory notably neglects ion-ion correlations,[19] which produce additional attractive contributions and increase the counterion density in the close vicinity of the polyion. Consequently, the PB equation underestimates the density of the high valence counterions close to the polyion.

In this article we present measurements based on anomalous small angle x-ray scattering[20] (ASAXS) to determine the distribution of small divalent counterions around high molecular mass HA under near-physiological conditions, i.e., where monovalent counterions are also present. Rubidium and strontium are used respectively to mimic the physiological monovalent ion sodium and divalent ion, calcium. In HA solutions, increasing the concentration of alkali earth metal ions such as calcium or strontium leads to the replacement of the sodium counterions. HA is a polymer of choice for this investigation, since, in contrast to the majority of synthetic and biological polyelectrolytes, its static structure is remarkably insensitive to the presence of calcium and it does not precipitate, even at high ionic strengths. Moreover, by virtue of its lower density and less complex structural hierarchy than DNA,[21,22] HA offers improved signal to noise ratio and is thus a more promising system for comparing experimental data with model counterion distributions. In principle, varying the wavelength of the incident x-ray beam in the vicinity of the absorption edge of the counterion yields information simultaneously on the distribution of ions and on the polymer.[20–28]

This paper is organized as follows. We begin by describing small angle neutron scattering (SANS) results obtained for HA solutions containing different combinations of mono- and divalent ions to determine the overall polymer structure in an extended length scale range and also to compare the effect of ions of different valencies and chemical nature. The ASAXS results for HA dissolved in rubidium chloride solution are then presented and the experimental findings compared with the predictions of the Poisson-Boltzmann model. The effect of divalent ions on the counterion distribution is then described in two different situations where monovalent cations are simultaneously present. In the first configuration (Ca^{++}/Rb^{+} system) the calcium ion is nonresonant (mute) at the incident x-ray energy, i.e., the ASAXS signal is due entirely to the rubidium ions. In the second case (Sr^{++}/Na^{+} system), sodium ions constitute the mute species, while strontium is the resonant species.

THEORY

ASAXS from polymer solutions

In polyelectrolyte solutions, the scattering intensity contains a contribution from the structure factor of the polymer as well as from that of the associated counterions.[20–28] Unlike the case of polyelectrolytes composed of low molecular weight monomers (e.g., polyacrylic acid), however, in large biopolymer molecules the number of counterions is a small fraction of the total atoms present. *A fortiori*, therefore, anomalous scattering from these counterions, which in turn involves only a small fraction of their electrons, contributes only marginally to the total scattering power. To determine the counterion distribution, three approaches may be envisaged to optimize the experimental conditions. First, the signal can be enhanced by investigating concentrated solutions.[21] Second, SAXS and SANS measurements on the same sample can be compared,[22] knowing that the relative contribution from the counterions in SANS is generally significantly smaller than in SAXS. Third, the counterion cloud can be modeled to fit the scattering data. In the present article the first of these approaches is not pursued owing to the high ionic strength needed in the solvent to compensate the polyion. The second approach provides useful information, although it calls for high accuracy in the measurements of absolute intensity. The route we adopt here is a combination of the second and third approaches.

The total scattering as a function of transfer wave vector $\mathbf{q}$ ($q=(4\pi/\lambda)[\sin(\theta/2)]$ where λ is the incident wavelength and θ the scattering angle) can be defined in terms of the electron density differences b_j between the solvent and each component j of the solution

$$I(q,E) = r_0^2[b_p^2 S_{pp}(q) + 2b_p \Re(b_c) S_{cp}(q) + \Re(b_c^2) S_{cc}(q)], \tag{1}$$

where r_0 (2.818×10^{-13} cm) is the classical radius of the electron, $b_p=(\rho_p-\rho_s)$ and $b_c=(\rho_c(E)-\rho_s)$ are the differences in electron density between the polymer (p) and solvent (s) and between the counterion cloud (c) and solvent, respectively, and $S_{jk}(q)$ are the partial structure factors, in which j and k represent either the polymer or the ion cloud. $\Re(x)$ denotes the real part of x. At the physiological conditions investigated here, the sodium and chlorine ions in the solution contribute negligibly to the electronic density of the bulk solvent, which can therefore be taken to consist of pure water. The electron density of water is

$$\rho_s = N_A Z/v_0, \tag{2a}$$

where N_A is Avogadro's number, $Z(=10)$ is the number of electrons in the water molecule, and v_0 is its molar volume. An equivalent expression holds for ρ_p, namely,

$$\rho_p = N_A Z_p d_p / M_p, \tag{2b}$$

where $Z_p(=199)$ and $M_p(=378)$ are the electron number and molar mass of the ionized HA repeating unit, while d_p is the mass density of the polymer. For the counterions, ρ_c is a complex quantity with a small imaginary component,

$$\rho_c(E) = [f_0 + f'(E) + if''(E)]/v_c. \tag{2c}$$

In this expression, the f_0, f', and f'' are, respectively, the energy-independent number of electrons, and the real and imaginary number of energy-dependent electrons in the counterion. The volume of the counterion, $v_c=4\pi r_c^3/3$, is defined by its radius r_c. In the vicinity of the absorption edge, f' and f'', and hence b_c, vary with the energy E of the incident x-ray beam: on increasing E below the absorption threshold, f' decreases while f'' increases. The contrast b_c between the counterions and the solvent thus varies, while that between polymer and solvent, b_p, remains constant. To evaluate the partial structure factors $S_{jk}(q)$, an estimate must first be made of the relative size of the different contrast coefficients b_j.

For the calculation of b_p we take for the density of HA $d_p=1.60$ g/cm^3, in agreement with values found in the literature.[29] This yields $b_p=1.73\times10^{23}$ e/cm^3. b_c is more complicated. In common with other workers,[24] we take the ionic radius r_c to be that obtained from crystallographic data. Although this assumption neglects the hydration layer surrounding the solvated ion, it is a useful basis for comparing the magnitudes of b. To proceed, we use the strontium ion as an illustration, bearing in mind that the results for rubidium turn out to be little different when adjusted for the appropriate energy range. For Sr^{++}, $f_0=36$, while the ionic radius is $r_c=1.12$ Å. At the reference energy used for strontium in this work, 15.8 keV, $f'=-3.38$ and $f''=0.54$.[30] Closer to the edge, at 16.102 keV, $f'=-7.72$ and $f''=1.43$. At $E=15.8$ keV these values yield $\Re(b_c)=5.21\times10^{24}$ e/cm^3 and $\Re(b_c^2)=2.71\times10^{49}$ e^2/cm^6. It follows that $b_c\gg b_p$.

The measurement of the intensity of the scattering spectrum of the same sample at two different energies E_1 and E_2 gives for the intensity difference

$$\Delta I(q,E_1,E_2)=I(q,E_1)-I(q,E_2)=2r_0^2[(\Delta f'/v_c)\{b_pS_{cp}(q)+(b_c-\Delta f'/2v_c)S_{cc}(q)\}+\{f''^2(E_2)-f''^2(E_1)\}S_{cc}(q)/2v_c^2], \quad (3)$$

where $\Delta f'=f'(E_1)-f'(E_2)$. For strontium ions at the energies under consideration, this may be expressed numerically as follows:

$$\Delta I(q,E_1,E_2)=2\times10^{46}r_0^2[7.4\{1.7S_{cp}(q)+(52.1-3.7)S_{cc}(q)\}+2.5S_{cc}(q)]. \quad (3b)$$

The last term in Eq. (3b), stemming from the imaginary part of the electron response, amounts to less than 1% of the total contribution to $S_{cc}(q)$, and can accordingly be neglected.

It has been shown[31] that under conditions of high q or low concentration, where intermolecular interactions are weak, the partial structure factors may be expressed as a product of the separate radial scattering amplitudes $a_j(q)$ of each component. Thus

$$S_{cp}(q)\propto a_c(q)a_p(q)/q$$

and

$$S_{pp}(q)\propto a_p(q)a_p(q)/q, \quad (4)$$

where the factor $1/q$ accounts for the linear nature of the chain. The expression for the scattering intensity at the reference energy E_1 thus becomes

$$I(q)=(r_0^2/q)[b_p^2a_p^2(q)+2b_pb_ca_c(q)a_p(q)+b_c^2a_c^2(q)]. \quad (5)$$

On setting $\Delta b=\Delta f'/v_c$, the amplitude of the counterion cloud can be expressed as

$$a_c(q)=\frac{\sqrt{q}}{r_0\Delta b}[\sqrt{I(q)}\pm\sqrt{I(q)-\Delta I(q)}]. \quad (6)$$

Since, physically, a_c and a_p must have the same sign, the negative solution is required. We may therefore define a relative amplitude $\alpha_c(q)$ of the counterion cloud

$$\alpha_c(q)=2r_0\Delta ba_c(q)/\sqrt{q}=\frac{\Delta I(q)}{\sqrt{I(q)}}\left[1-\frac{\Delta I(q)}{4I(q)}+\cdots\right]. \quad (7)$$

Insofar as $\Delta I(q)/I(q)\ll1$, this yields

$$\alpha_c(q)=\Delta I(q)/[I(q)]^{1/2}, \quad (8)$$

in which the E_1 and E_2 implicit in this equation are respectively the reference energy measured far below the absorption edge and that just below the edge, where the anomalous effects are most pronounced.[15,31] Use of high molecular weight polymers above the overlap concentration ensures that the chain fractions between entanglements are locally rodlike over a length exceeding the counter-ion cloud thickness and that they possess a large number of charged subunits.

Small angle neutron scattering

SANS measurements yield information complementary to that of SAXS. Owing to the longer wavelength of the neutron beam, smaller values of transfer wave vector q can be explored, thus probing any larger scale structures that may be present in the system. Furthermore, SANS measurements allow corroboration of the SAXS results, particularly to verify that the signal below the absorption threshold is not perturbed by residual ionic effects, and determination of structural changes in an extended range of q vectors, i.e., in the present study the equivalence of strontium and calcium ions as well as that of rubidium and sodium.

For SANS, an expression similar to Eq. (1) holds, but the contrast factors are defined in terms, not of the electron density, but of the neutron scattering length density of the solvent and the polymer or the counterion environment.[32] In this case, the scattering intensity is dominated by the first term in Eq. (1) because the contribution from the nuclei of the ions is weak. Thus, making SANS and ASAXS measurements on the same polymer sample provides a valuable means of discriminating between the signals arising, on the one hand, from the polymer structure alone and, on the other hand, from the counterion cloud.

It has previously been observed that the scattering response of semidilute high molecular weight neutralised polyelectrolyte solutions behaves similarly to a set of interconnected rods of length L and of cross-sectional radius r_c.[33] Furthermore, at small values of q the scattering response from polyelectrolyte solutions is generally dominated by additional scattering from the surfaces of large domains, displaying a power law dependence. Thus

$$I(q)=\Delta\rho^2\frac{k_BT\varphi^2}{K_{os}}\frac{1}{(1+qL)(1+q^2r_c^2)}+Aq^{-s}, \quad (9)$$

where $\Delta\rho$ is the neutron contrast between polymer and solvent, k_B is the Boltzmann constant, T is the absolute temperature, K_{os} is the osmotic modulus, and φ is the polymer volume fraction. The exponent s $(3<s\leqslant4)$ describes the scattering from the surface of the large domains.

TABLE I. Sample composition.

HA % (w/w)	NaCl (mM)	RbCl (mM)	$CaCl_2$ (mM)	$SrCl_2$ (mM)	Abbreviation
4(SAXS, SANS)	100	0	0	0	NaHA
4	100	0	0	10	NaHASr10
4	100	0	0	30	NaHASr30
4	100	0	0	50	NaHASr50
4 (SAXS, SANS)	100	0	0	100	NaHASr100
4 (SAXS, SANS)	0	100	0	0	RbHA
4	0	100	10	0	RbHACa10
4	0	100	20	0	RbHACa20
4	0	100	30	0	RbHACa30
4	0	100	50	0	RbHACa50
4	0	100	100	0	RbHACa100
4 (SAXS, SANS)	100	0	100	0	NaHACa100

EXPERIMENTAL SECTION

Materials and methods

Sample preparation

Solutions of sodium hyaluronate (HA, Sigma $M_w = 1.2 \times 10^6$, $M_w/M_n = 1.5$) were prepared in H_2O containing 100 mM NaCl. SANS measurements were made in a 92% H_2O/8% D_2O v/v mixture. For this solvent the mean scattering length density is zero. To optimize the signal, the solutions were prepared at 4% (w/w) HA. Above this concentration, HA solutions exhibit physical gelation, even in the absence of divalent cations. The sodium chloride concentration and *p*H(=7) were identical in all samples. The RbHA samples were prepared by first dissolving HA in a 100 mM RbCl aqueous solution. This solution was then dialyzed against a 100 mM RbCl solution to remove the sodium ions. Monovalent ion concentrations were set at 100 mM, either with RbCl or NaCl (denoted RbHA and NaHA, respectively). Divalent salt concentrations, $CaCl_2$ or $SrCl_2$ (RbHACa/NaHASr), were varied in the range of 0–100 mM. The use of the same anion throughout, Cl^-, minimized the number of participating chemical components. The solutions were allowed to come to equilibrium, as determined from the intensity of the static light scattering signal (two to three days). Table I lists the composition of the samples investigated in the ASAXS measurements, as well as those probed by SANS.

ASAXS

The ASAXS measurements were made on the BM2 beam line at the European Synchrotron Radiation Facility (ESRF). The resolution of the two-dimensional (2D) charge coupled device (CCD) detector was 50 μm. Corrections were made for dark counts and camera distortion. The measured intensities were normalized using a standard polyethylene sample (Lupolen) of known scattering cross section. The transfer wave vector range explored was $0.008\ \text{Å}^{-1} \leqslant q \leqslant 1.0\ \text{Å}^{-1}$. The upper limit $q_{\max}$ defines the spatial resolution that can be achieved in this type of measurement. To limit radiation damage effects, sequences of exposure times were limited to 20 s and the position of the beam in the sample was changed at each successive energy. No detectable radiation damage effects were found in any of the samples.

At the high values of q explored in this investigation, solvent background corrections are of paramount concern, particularly owing to the fluorescent signal generated close to the absorption edge. The background correction procedure followed here consisted in subtracting the signal from a solution having the same ionic composition and concentration as the sample. To maintain the sample thickness identical as closely as possible to that of the background solution, the specimens were held between mica windows of thickness 25 μm separated by a 2 mm Teflon washer. Residual differences in thickness appeared in the form of an additional fluorescent background that was corrected by subtracting a small q-independent intensity (approximately 1% of the background) from the base line. The SAXS measurements were made at six energies below the absorption edge (15.1997 keV) of rubidium: 14.900, 15.08, 15.15, 15.18, 15.193, and 15.197 keV and at six energies below the absorption edge (16.1046 keV) of strontium: 15.800, 15.984, 16.056, 16.085, 16.097, and 16.102 keV.

SANS

The SANS measurements were made on the NG3 instrument at the National Institute of Standards and Technology at an incident wavelength of 8 Å. The explored wave vector range was $0.003\ \text{Å}^{-1} \leqslant q \leqslant 0.15\ \text{Å}^{-1}$. After azimuthal averaging of the SANS spectra, corrections for detector response, cell windows, and incoherent scattering were applied.

RESULTS AND DISCUSSION

SANS

SANS yields information on the structure of the polymer in solution and its variation due to changes in the interaction with the surrounding molecules. In solutions of charged polymers, the conformation is governed by electrostatic forces. In general, changes in the ionic environment (ion valence, ion concentration, etc.) modify the polymer organization, which are therefore reflected in the scattering response. Figure 1 shows the combined SANS and SAXS responses of the 4% HA solutions in different ionic environments. The SAXS spectra from the RbHA and NaHA solutions were measured at 14.900 keV and those of NaHACa100 and NaHASr100 at 15.8 keV. Both of these responses correspond to

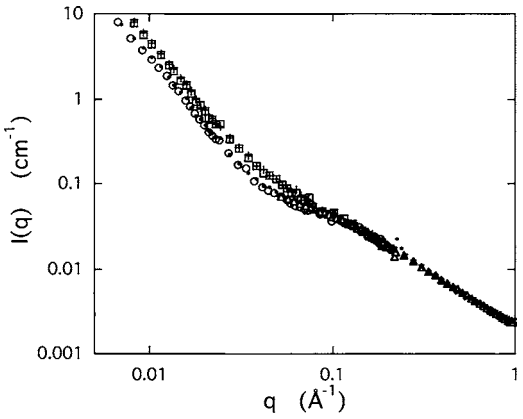

FIG. 1. Scattering spectra (in SAXS intensity units) of 4% HA solutions containing 0 mM $CaCl_2$ and 100 mM NaCl SANS (●), 100 mM RbCl SANS (○) and 100 mM RbCl SAXS at 14.9 keV (△). Also shown are HA solutions in 100 mM NaCl containing 100 mM $CaCl_2$ SANS (+), 100 mM $SrCl_2$ SANS (□), and 100 mM $SrCl_2$ SAXS at 15.8 keV (×).

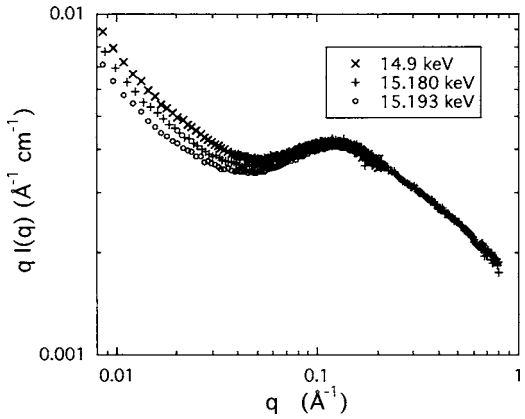

FIG. 2. Plot of $qI(q)$ for 4% solutions of divalent ion-free RbHA solutions at three different incident x-ray energies below the Rb threshold. For the region $q>0.2$ Å^{-1} the data from the three spectra are indistinguishable in the resolution of this figure. For clarity, only 20% of the data points are plotted.

energies at which anomalous scattering effects can be considered negligible. The SANS and SAXS data overlap, and in this region the intensities are in excellent agreement. The spectra from the NaHA and RbHA solutions, containing respectively 100 mM NaCl and 100 mM RbCl, are identical within the experimental uncertainty. The same is true for the spectra from the NaHACa100 and NaHASr100 solutions containing 100 mM NaCl with either 100 mM $CaCl_2$ or 100 mM $SrCl_2$. As far as the polymer structure is concerned, therefore, it can be concluded that sodium and rubidium ions, on the one hand, and calcium and strontium ions, on the other, are mutually equivalent. In the region $q>0.1$ Å^{-1}, where the scattering is defined principally by the cross-sectional radius of the polymer chain, the scattering curves from all the samples converge and decrease quasilinearly. Close to 0.1 Å^{-1} a shoulder is apparent, below which a strong upturn in the intensity occurs. The latter is a common feature in polyelectrolyte solutions and is usually attributed to domain formation. In this region, the spectra of the solutions with divalent ions differ from those containing monovalent ions alone. In Fig. 1 the calculation of the scattering contrasts was obtained, assuming 1.60 g/cm^3 for the density of HA, as in the calculation of the electron density contrast. Residual differences between the SANS and SAXS intensities were less than 5% and were corrected by a simple normalization factor.

The weak variation of the shape of the scattering curves with ionic composition in the high-q region with an ionic composition is favorable for ASAXS observations, in which the scattering from the ions must be separated from that of the polymer.

ASAXS measurements in HA solutions with Rb ions

Monte Carlo and molecular dynamics simulations have shown that in polyelectrolyte solutions divalent cations are concentrated in the vicinity of the negatively charged polymer chain, while monovalent cations, which form a more extended ion cloud, tend to move virtually freely throughout the entire solution. In mixtures of mono- and divalent cations, however, the situation is more complicated, since the ion distribution is perturbed by the exchange of the monovalent by the divalent counterions. This condition is of particular importance in biological systems, where charged macromolecules are exposed to an environment containing both sodium and calcium ions.

In this section we investigate the distribution of monovalent ions in the HA solutions in the absence of divalent ions. The concentration of the monovalent salt, in this case rubidium chloride, is set at 100 mM. In this solution, as under physiological conditions, the HA molecules are fully dissociated. The conditions investigated all correspond to those under which the Manning theory predicts counterion condensation.[13] The characteristic length scale for the ion cloud distribution is its cross-sectional radius. To evaluate these short characteristic distance scales, ASAXS measurements extending to $q\approx 1$ Å^{-1} are therefore necessary.

As already stated, the intensity of the anomalous scattering component is small. Figure 2 shows the signal from a RbHA solution at three different energies, 14.9, 15.180, and 15.193 keV. The data are plotted in the representation $qI(q)$ vs q in order to reduce the vertical scale and make the differences more visible. As the incident x-ray energy increases towards the absorption edge of rubidium, the change in effective electron number of the resonant ions decreases more markedly towards its minimum value, and the intensity from RbHA accordingly decreases. As expected, therefore, at low q the higher energy measurements lie below the spectrum measured at 14.9 keV. At the high q end of the spectrum, however, the differences among the responses tend to vanish.

As indicated in the theoretical section, the scattering amplitude of the radial distribution of the ions is governed by the difference between the spectra measured at two energies, normalized by the square root of the reference signal. The resulting scattering amplitude $\alpha_c(q)$ is the Fourier transform of the corresponding ion cloud, and its functional form reflects the shape and radial extent of the counterion distribution. Note that since the amplitude $\alpha_c(q)$ is the square root of an intensity, its units are expressed in cm$^{-1/2}$. In Fig. 3 data set (a) accordingly shows the normalized SAXS amplitude $\alpha_{Rb}(q)$ from Eq. (8) for the RbHA solution, where $E_1=14.9$ keV and $E_2=15.197$ keV. At low q the amplitude

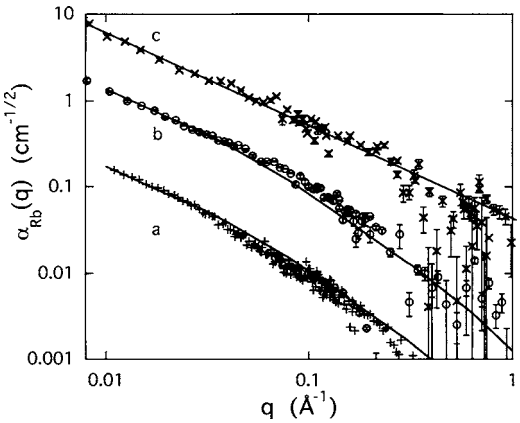

FIG. 3. Plot of normalized SAXS scattering amplitude $\alpha_{Rb}(q)$ with $E_1=14.900$ keV and $E_2=15.196$ keV from RbHA solutions containing (a) 0 mM $CaCl_2$ (+), (b) 50 mM $CaCl_2$ (○), and (c) 100 mM $CaCl_2$ (×). Successive data sets are shifted upward by one decade. Continuous lines in (a) and (b) are the solution of the Poisson-Boltzmann equation for monovalent counterions [Eq. (10)]. In (c), the straight line is a guide for the eye. To reduce scatter the data in the figure are binned, the vertical bars displayed being the standard errors of the regrouping procedure.

$\alpha_{Rb}(q)$ follows a power law with exponent −1, which is greater than that (−1/2) expressed in Eq. (7). This discrepancy is not due to neglect of the higher order terms in Eq. (8), as the difference between the two expressions is too small to be distinguishable in Fig. 3. While it is conceivable that the stronger than expected slope is related to intermolecular effects due to the finite concentration of the solution, its insensitivity to ionic strength suggests otherwise. For the present purposes, however, it is not the power law (which possesses no intrinsic length scale) itself but deviations from power law behavior that are important, since these express the radial component of the distribution. The continuous downturn of the curve with increasing q is thus the footprint of the resonant counterion cloud surrounding the polymer chains.

The results in Fig. 3(a) may be compared with theoretical estimates of the ion density distribution $\rho(r)$. The radial amplitude term $a_c(q)$ of Eq. (6) can be deduced from a model in which the counterions are confined in cylindrical cells of radius R, the size of which is defined by the polymer concentration.[31] The observed amplitude $\alpha_c(q)$ appearing in Eq. (7) is then given by the two-dimensional Fourier transform

$$\alpha_c(q) \propto \frac{a_c(q)}{q} = \frac{1}{q}\int_0^R 2\pi r J_0(qr)\rho(r)dr, \tag{10}$$

where $J_0(qr)$ is the cylindrical Bessel function of order zero. [In Eq. (10), for conformity with the present experimental observations, the amplitude α_c is divided by q rather than by $q^{1/2}$.] For monovalent ions, the radial concentration profile $\rho(r)$ is conveniently modeled by the Poisson-Boltzmann distribution.[34,35] The continuous line through data set (a) of Fig. 3 shows that the shape of the resulting calculated scattering amplitude is in reasonable agreement with the experimental results. An estimate of the numerical value of the radius of gyration of this cloud, obtained by fitting a Guinier expression to the experimental data in region $q<0.06$ Å^{-1}, yields $r_G=15\pm2$ Å. On taking the cross-sectional radius of the HA molecule $n_0=5.2$ Å, this finding indicates that the effective thickness of the counterion cloud is approximately 10 Å.

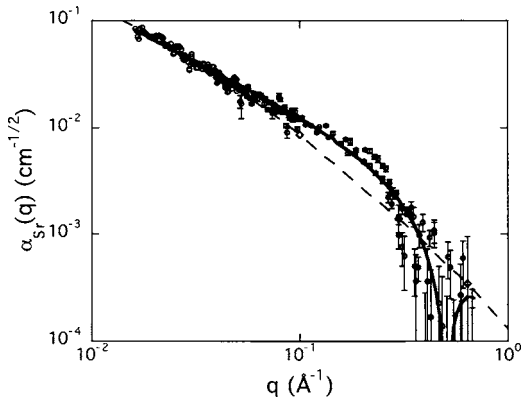

FIG. 4. Plot of $\alpha_{Sr}(q)$ with $E_1=15.8$ keV and $E_2=16.102$ keV for sample NaHASr100. In the higher q range the data points are binned to reduce statistical noise. The continuous line is Eq. (11) with $r_c=7.5$ Å. The dashed line is the Poisson-Boltzmann curve for comparison [Eq. (10)].

ASAXS measurements in HA solutions containing both mono- and divalent ions

Since charged polymers preferentially adsorb multivalent ions,[36,37] the electrostatic potential experienced by the displaced monovalent cations is strongly screened and the simple Poisson-Boltzmann model is no longer valid. Although several direct experimental observations either of monovalent ions or of divalent ions alone have been reported,[20–28,30] these results are not necessarily relevant when both species are simultaneously present. To investigate the ion distribution in the presence of divalent ions, we evoke two different configurations. In the first, the sample contains 100 mM NaCl with varying amounts of $SrCl_2$ (NaHASr10 to NaHASr100). For these samples, the divalent ion distribution is determined by performing a set of ASAXS measurements at different energies below the absorption edge of strontium. In the second configuration, the system contains 100 mM RbCl together with varying amounts of $CaCl_2$ (RbHACa10 to RbHACa100). Here, the ASAXS measurements probe the monovalent cation cloud.

Figure 4 shows the SAXS amplitude $\alpha_{Sr}(q)$ of the strontium signal for NaHASr100, obtained in the same way as described above. The defining energies are $E_1=15.8$ keV and $E_2=16.102$ keV. As the rubidium case, at low q the data obey a power law with exponent −1. At high q, however, a strong downturn is observed. It is qualitatively different from the scattering response of the RbHA solution in the absence of divalent ions [Fig. 3(a)]. The shape of the NaHASr100 response curves (as well as those of lower strontium concentration) resembles instead that of a cylinder having a well defined cross-sectional radius. This finding implies that the strontium ions lie close to the polyanion. To model the measurements in a manner consistent with the previous results, the data are fitted to the expression for the scattering amplitude of a solid cylinder of radius r_c, together with a factor q^{-1}, i.e.,

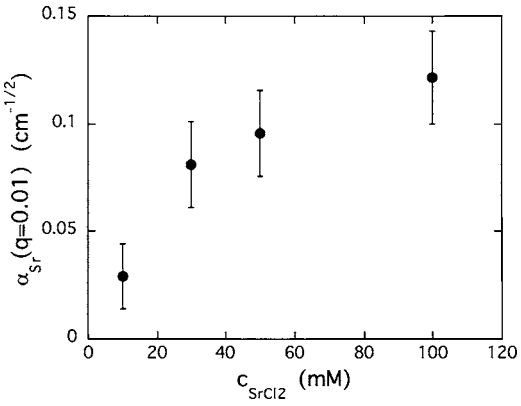

FIG. 5. Scattering amplitude $\alpha_{Sr}(q=0.01)$ of Sr^{++} anomalous signal at $q=0.01$ Å^{-1} as a function of the $SrCl_2$ concentration of the solution.

$$\alpha_{Sr}(q) \propto q^{-1}\left|\frac{2J_1(qr_c)}{qr_c}\right|, \tag{11}$$

where $J_1(qr_c)$ is the cylindrical Bessel function of order 1. The continuous line in Fig. 4 is the resulting fit. The values found for r_c are 7.5 ± 1.0 Å for all the strontium chloride concentrations studied. This result is appreciably greater than the effective cross-sectional radius found for HA from SANS ($r_0\approx5.2$ Å) and corroborates the conclusion that the Sr counterions move in the close vicinity of the polymer backbone. The finding is consistent not only with ASAXS results on another stiff polyelectrolyte molecule, DNA, where the divalent cations were also found to remain close to the polyanion, even in conditions of excess monovalent ions,[22] but also with measurements performed with divalent ions alone.[16,21] For comparison, the dashed curve shown in this figure is the amplitude $\alpha_m(q)$ for the monovalent case, i.e., the Poisson-Boltzmann distribution of Fig. 3(a).

The anomalous scattering amplitude $\alpha_{Sr}(q)$, measured at $q=0.01$ Å^{-1}, is shown in Fig. 5 as a function of the $SrCl_2$ content. At this value of q, where the asymptotic power law regime is recovered, the different amplitudes $\alpha_{Sr}(q)$ may legitimately be compared. Although the estimated errors are large, the effect of saturation in the divalent-monovalent ion exchange process is clearly visible. These findings are closely analogous to the phenomenon of calcium saturation, measured by elemental analysis of the calcium-sodium exchange in polyacrylic acid gels.[38]

We now turn to the second configuration, in which resonant monovalent counterions coexist with mute divalent cations. In this case ASAXS measurements are made on complementary samples in which rubidium is the monovalent and calcium the divalent ion. The amplitude factor $\alpha_{Rb}(q)$ is then insensitive to the scattering intensity of the calcium and reflects only the rubidium ion distribution. The resulting values of $\alpha_{Rb}(q)$ for RbHASr50 and RbHASr100 are compared in Fig. 3 [data sets (b) and (c)], along with the corresponding divalent ion-free sample RbHA (a). For clarity, each successive data set in this figure has been shifted vertically by one decade. The continuous line through the RbHASr50 data, which is the same as that for RbHA, adjusted for the different amplitudes, shows that the Poisson-Boltzmann fit is poorer when divalent ions are present.

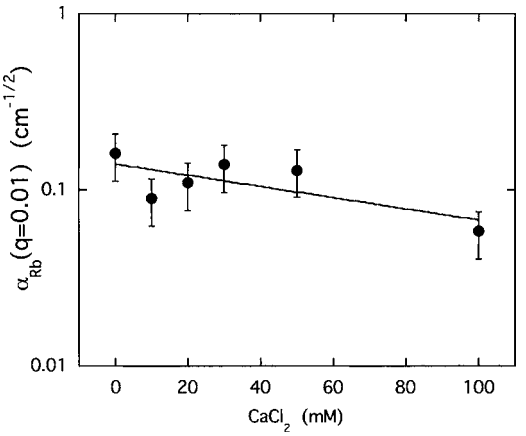

FIG. 6. Scattering amplitude $\alpha_{Rb}(q)$ of anomalous Rb^+ signal as a function of the $CaCl_2$ content of the solution.

An inspection of Fig. 3 reveals two important features. First, the characteristic curvature of $\alpha_{Rb}(q)$, which describes the extent of the monovalent ion cloud, gradually disappears, giving way to practically straight line behavior at 100 mM $CaCl_2$. Its amplitude also decreases. These results imply that the thickness of the rubidium ion cloud decreases with increasing calcium concentration; i.e., the radial distribution of the counterions crowds closer to the axis. This observation is consistent with a reduction of the Debye-Hückel screening length with increasing ionic strength in the solution. Second, although the amplitude of the $\alpha_{Rb}(q)$ curves decreases with increasing calcium content, it does not vanish. Even when the divalent ion content exceeds the stoichiometric concentration by more than an order of magnitude, the monovalent counterion cloud is still detectable. Figure 6 shows the variation of $\alpha_{Rb}(q)$ for rubidium as a function of calcium content. Although the data are subject to experimental noise, $\alpha_{Rb}(q)$ appears as a weakly decreasing function of calcium content. The straight line through the data in this figure is an exponential decay with an attenuation coefficient defined by a characteristic $CaCl_2$ concentration equal to 140 mM.

The schematic diagram of Fig. 7 summarizes the findings of this investigation. In the absence of divalent ions, the

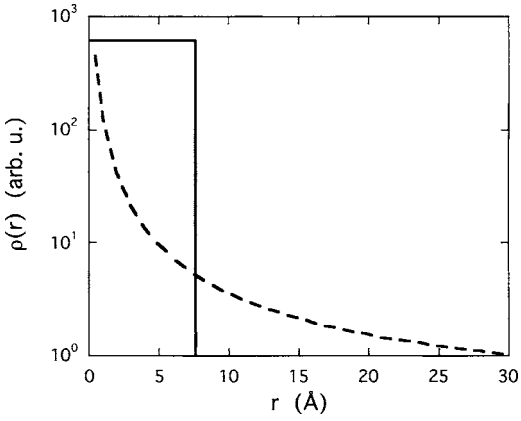

FIG. 7. Schematic diagram of counterion density $\rho(r)$ around the HA chain as a function of radius r. Continuous line, cylindrical shell model for divalent ions; dashed line, Poisson-Boltzmann distribution for monovalent ions. With increasing divalent ion concentration $\rho(r)$ of the monovalent ions decreases in width and in amplitude.

distribution of monovalent counterions follows a Poisson-Boltzmann law as a function of radial distance r, illustrated by the dashed curve of the figure. The presence of divalent ions causes the monovalent counterion distribution to move closer to the axis. In contrast, divalent counterions always move in close proximity to the polymer chain, with a radial distribution function that can be approximated by a cylindrical shell around the polymer chain (continuous line).

CONCLUSIONS

Anomalous SAXS measurements are used to probe the ion cloud distribution in semidilute solutions of hyaluronic acid containing both mono- and divalent cations in the presence of added salt. The ionic conditions prevailing in physiological systems were mimicked by using rubidium or strontium ions in place of sodium and calcium. SANS measurements ascertained that this ion substitution causes no detectable changes in the structure of the HA solution. The main findings are as follows.

(1) In the absence of divalent ions, the shape of the anomalous scattering amplitude $\alpha_c(q)$ is consistent with the ion distribution calculated from the Poisson-Boltzmann equation, as has been found by other workers.
(2) In monovalent-divalent ion mixtures, divalent counterions preferentially occupy the immediate vicinity of the charged polyanion. This finding is in agreement with results reported for DNA solutions in the presence of mono and divalent counterions.[22] The effective radius of the divalent ion sheath is 7.5 ± 1.0 Å.
(3) The amplitude of the divalent ion signal tends to saturate at high divalent ion content.
(4) Both the effective diameter and the amplitude of the monovalent ion cloud decrease with increasing divalent ion concentration. Even in a large excess of divalent ions, ion exchange is incomplete.

ACKNOWLEDGMENTS

We are grateful to the European Synchrotron Radiation Facility for access to the French CRG x-ray beam line BM2 as well as to the National Institute of Standards and Technology, U.S. Department of Commerce in providing the neutron research facilities used in this experiment. This work is based on activities supported by the National Science Foundation under Agreement No. DMR-942310. We extend our thanks to Boualem Hammouda and Jean-François Bérar for their invaluable help. This research was supported by the Intramural Research Program of the NICHD/NIH.

[1] B. Alberts, A. Johnson, J. Lewis, M. Raff, K. Roberts, and P. Walter, *Molecular Biology of the Cell*, 4th ed. (Garland, New York, 2002), Chap. 19.
[2] A. G. Ogston and J. E. Stainer, J. Physiol. (London) **199**, 244 (1953).
[3] E. L. Radin, D. A. Swann, and P. A. Weisser, Nature (London) **228**, 377 (1970).
[4] M. Benz, N. Chen, and J. Israelachvili, J. Biomed. Mater. Res. **71A**, 6 (2004).
[5] R. L. Cleland, Arch. Biochem. Biophys. **180**, 57 (1977).
[6] I. Rosenberg, W. Hellmann, and A. K. Kleinschmidt, J. Biol. Chem. **245**, 4123 (1970).
[7] M. K. Cowman, D. M. Hittner, and J. Feder-Davis, Macromolecules **29**, 2894 (1996).
[8] N. Meechai, A. M. Jamieson, J. Blackwell, D. A. Carrino, and R. Bansal, J. Rheol. **46**, 685 (2002).
[9] M. J. Stevens, Phys. Rev. Lett. **82**, 101 (1999).
[10] M. J. Stevens, Biophys. J. **80**, 130 (2001).
[11] C. N. Patra and A. Yethiraj, J. Phys. Chem. B **103**, 6080 (1999).
[12] Y. Zhang, J. F. Douglas, B. D. Ermi, and E. Amis, J. Chem. Phys. **114**, 3299 (2001).
[13] G. S. Manning, J. Chem. Phys. **51**, 934 (1969).
[14] F. Oosawa, *Polyelectrolytes* (Dekker, New York, 1971).
[15] J. R. C. van der Maarel, L. C. A. Groot, M. Mandel, W. Jesse, G. Jannink, and V. Rodriguez, J. Phys. II **2**, 109 (1992).
[16] M. Patel, S. Rosenfeldt, M. Ballauff, N. Dingenouts, D. Pontoni, and T. Narayanan, Phys. Chem. Chem. Phys. **6**, 2962 (2004).
[17] Sz.-L. Chang, S.-H. Chen, R. L. Rill, and J. S. Lin, J. Phys. Chem. **94**, 8025 (1990).
[18] R. Kjellander and S. Marcelja, Chem. Phys. Lett. **112**, 49 (1984).
[19] M. Deserno, C. Holm, and S. May, Macromolecules **33**, 199 (2000).
[20] C. E. Williams, in *Neutron, X-Ray and Light Scattering*, edited by P. Lindner and T. Zemb (Elsevier, New York, 1991).
[21] R. Das, T. T. Mills, L. W. Kwok, G. S. Maskel, I. S. Millet, S. Doniach, K. D. Finkelstein, D. Herschlag, and L. Pollack, Phys. Rev. Lett. **90**, 188103 (2003).
[22] I. Morfin, F. Horkay, P. J. Basser, F. Bley, A.-M. Hecht, C. Rochas, and E. Geissler, Biophys. J. **87**, 2897 (2004).
[23] I. Sabbagh, M. Delsanti, and P. Lesieur, Eur. Phys. J. B **12**, 253 (1999).
[24] B. Guilleaume, J. Blaul, M. Ballauff, M. Wittemann, M. Rehahn, and G. Goerigk, Eur. Phys. J. E **8**, 299 (2002).
[25] I. Morfin, F. Horkay, P. J. Basser, F. Bley, F. Ehrburger-Dolle, A.-M. Hecht, C. Rochas, and E. Geissler, Macromol. Symp. **200**, 227 (2003).
[26] N. Dingenouts, R. Merkle, X. Guo, T. Narayanan, G. Goerigk, and M. Ballauff, J. Appl. Crystallogr. **36**, 578 (2003).
[27] G. Goerigk, R. Schweins, K. Huber, and M. Ballauff, Europhys. Lett. **66**, 331 (2004).
[28] A. Jusufi and M. Ballauff, Macromol. Theory Simul. **15**, 193 (2006).
[29] S. Hokputsa, K. Jumel, C. Alexander, and S. E. Harding, Carbohydr. Polym. **52**, 111 (2003).
[30] D. T. Cromer and D. A. Libermann, Acta Crystallogr., Sect. A: Cryst. Phys., Diffr., Theor. Gen. Crystallogr. **A37**, 267 (1981).
[31] S. S. Zakharova, S. U. Egelhaaf, L. B. Bhuiyan, C. W. Outhwaite, D. Bratko, and J. R. C. van der Maarel, J. Chem. Phys. **111**, 10706 (1999).
[32] V. F. Sears, Neutron News **3**, 26 (1992).
[33] F. Horkay, A.-M. Hecht, I. Grillo, P. J. Basser, and E. Geissler, J. Chem. Phys. **117**, 9103 (2002).
[34] T. Alfrey, P. W. Berg, and H. Morawetz, J. Polym. Sci. **7**, 543 (1951).
[35] R. M. Fuoss, A. Katchalsky, and S. Lifson, Proc. Natl. Acad. Sci. U.S.A. **37**, 579 (1951).
[36] M. Muthukumar, J. Chem. Phys. **105**, 5183 (1996).
[37] M. Muthukumar, J. Chem. Phys. **120**, 9343 (2004).
[38] F. Horkay, I. Tasaki, and P. J. Basser, Biomacromolecules **2**, 195 (2001).